Interfacial properties deduced from nucleation experiments: A Cahn–Hilliard analysis

László Gránásy, Tamás Pusztai, and Peter F. James

Citation: The Journal of Chemical Physics **117**, 6157 (2002); doi: 10.1063/1.1502652
View online: http://dx.doi.org/10.1063/1.1502652
View Table of Contents: http://scitation.aip.org/content/aip/journal/jcp/117/13?ver=pdfcov
Published by the AIP Publishing

Interfacial properties deduced from nucleation experiments: A Cahn–Hilliard analysis

László Gránásy[a] and Tamás Pusztai
Research Institute for Solid State Physics and Optics, P.O.B. 49, H-1525 Budapest, Hungary

Peter F. James
Department of Engineering Materials, Glass Research Centre, The University of Sheffield, Sir Robert Hadfield Building, Mappin Street, Sheffield S1 3JD, United Kingdom

(Received 26 February 2002; accepted 2 July 2002)

We apply a single-order-parameter Cahn–Hilliard theory to deduce properties of the fluid–crystal interface from nucleation experiments: The two Cahn–Hilliard parameters (the free energy scale and the coefficient of the square-gradient term) are chosen so that the experimentally determined interfacial free energy of nuclei is recovered. The theory is then used to predict the thickness and free energy of the equilibrium planar interface, and other quantities such as the Tolman length and characteristic thickness, which describe the curvature dependence of the interfacial free energy. The accuracy of the method is demonstrated on systems (Lennard-Jones and ice-water) for which these properties are known. Experimental data available for five stoichiometric oxide glasses are then analyzed. The reduced interfacial free energy (Turnbull's α) and the interface thickness, we obtained, cover the $\alpha=0.28-0.51$ and the $d=0.8-1.6$ nm ranges. For oxide glasses we find that α scales with $n^{-1/3}$, where n is the number of molecules per formula unit. In agreement with computer simulations, the Tolman length is strongly size dependent, while far weaker though still perceptible temperature dependence is observed for the characteristic interface thickness used in Gránásy's phenomenological diffuse interface theory. In some cases bulk crystal properties prevail at the center of nuclei, while in other systems the nuclei are ramified, and the local properties significantly deviate from those of the macroscopic crystal. The accuracy of these results rests on a hypothesized temperature independence of the Cahn–Hilliard parameters, an assumption whose validity remains to be seen at large undercoolings. © *2002 American Institute of Physics.*
[DOI: 10.1063/1.1502652]

I. INTRODUCTION

Computer simulations[1–5] and experiments[6] performed in the past decades revealed that the crystal–liquid interface is diffuse on the molecular scale: The transition from bulk liquid to bulk solid takes place in a region that extends to several molecular layers. Advanced models, which rely on the density functional technique, reproduce this feature well.[7] Owing to the experimental and theoretical difficulties direct information is unavailable for the crystal–liquid interface of complex systems. Therefore, indirect approaches, which have the potential to deduce such information from experiment with some accuracy, are of importance.

Information on the crystal–liquid interface plays a central role in understanding the initial stage of crystallization, called nucleation, during which crystal-like fluctuations from via stochastic processes. Those fluctuations whose size exceeds that of the critical fluctuation (nucleus), determined by the interplay of the interfacial and volumetric contributions to the excess free energy, have a good chance to reach macroscopic dimensions, while the smaller ones decay with a high probability. Nucleation experiments performed in undercooled liquids proved one of the indispensable sources of interfacial information. The measurement of maximum undercooling and the study of nucleation kinetics on droplet emulsions were the first methods, which demonstrated that a substantial excess free energy is associated with the crystal–liquid interface.[8] Unfortunately, the accuracy of these methods is hampered by various factors. For example, the formation of crystalline fluctuations may be assisted by heterogeneities in the system (impurities, foreign particles, surfaces, container walls). Some of these difficulties can be avoided by applying advanced experimental methods that rely on melt dispersion (division of the melt into such small droplets that only a negligible fraction contains heterogeneities) or containerless processing.[9] A wealth of nucleation data is available for oxide glasses, which are especially suitable for studying nucleation kinetics.[10,11] While reasonably accurate nucleation data became available in the past decades, and methods have been developed to test whether homogeneous or heterogeneous nucleation took place in the experiment,[8–12] little has been done to utilize recent advances of nucleation theory for improving the evaluation of experimental results. With a few exceptions[12] the experiments are evaluated using the classical nucleation theory developed by Turnbull and Fisher.[13] In describing crystalline fluctuations (clusters) they use the droplet model, which relies on the bulk interfacial and crystal properties in calculat-

[a]Author to whom correspondence should be addressed; electronic mail: grana@szfki.hu

ing the excess free energy. In the light of the typical size of nuclei (few times ten to a few times hundred molecules) and the diffuse crystal–liquid interface, the accuracy of this approach is questionable. Indeed, in cases where accurate input data and nucleation rates are available (vapor condensation and Ising model), the classical nucleation theory fails.[14,15] Various phenomenological approaches have been proposed to remove these discrepancies.[16–22] Of them, the continuum models (Cahn–Hilliard/density functional/phase field theories) are able to describe a position dependent change of local state across the interface.[17,20–22] These offer the possibility of deducing detailed interfacial information from nucleation experiments.

In this paper, we make the first step in this direction, and use a single-order-parameter Cahn–Hilliard approach to evaluate interfacial information from homogeneous nucleation experiments available in the literature. The rest of the paper is organized as follows: In Sec. II, we describe the model and the strategy of evaluating interfacial information. The nucleation data and physical properties are specified in Sec. III. The interfacial data are presented and discussed in Sec. IV. Finally, the results are summarized, and a few concluding remarks are made in Sec. V.

II. INTERFACIAL PROPERTIES FROM NUCLEATION EXPERIMENT

In this section we briefly summarize the models used in evaluating interfacial properties from nucleation experiments. Any nucleation theory developed to date consists of a kinetic and a thermodynamic part. The former describes the growth and decay of crystalline fluctuations on the basis of the free energy surface of fluctuations provided by the latter. There are essentially two approaches to the kinetic part: (a) The classical kinetic model by Turnbull and Fisher,[13] which relies on single molecule attachment and detachment processes and was generalized to include cluster coagulation by several authors;[23] and (b) the general field theoretical formulation by Langer[24] that has been adopted for crystal nucleation by Grant and Gunton[25] and Roy *et al.*[26] Recent work by Bartell and co-workers show that these approaches lead to considerably different results.[27] It is worth mentioning, however, that the results by Grant and Gunton refer to systems where the heat transport is the rate-limiting factor. This situation is expected to occur in simple liquids. In complex liquids and glasses treated here, nucleation and crystal growth scale rather with the self diffusion of the constituent molecules. Unlike the field theoretic models, the classical kinetic approach has been extensively tested under such conditions, and was found to be in remarkable agreement with experiment.[28] Therefore, we adopt the classical kinetic approach to describe the growth and decay of crystalline fluctuations.

A. Classical kinetic approach

In describing the time evolution of cluster population, only single molecule attachment and detachment are considered. The respective master equations read as[10,13,28]

$$dN_i/dt = D_{i+1}N_{i+1} + A_{i-1}N_{i-1} - (D_i + A_i)N_i, \qquad (1)$$

where N_i is the number density of i-mers, $i \geqslant u$, u is the minimum cluster size treated numerically, while A_i and D_i are the rates of single molecule attachment and detachment, related via the detailed balance as

$$0 = A_i N_{\mathrm{eq},i} - D_{i+1} N_{\mathrm{eq},i+1}. \qquad (2)$$

The number densities in the respective constrained equilibrium follow the Boltzmann distribution $N_{\mathrm{eq},i} = N_L \exp\{-W_i/kT\}$, where W_i is the free energy of formation of the i-mer, k the Boltzmann's constant, and N_L is the number density of molecules in the liquid. As a consequence of Eq. (2), only the attachment rate A_i needs to be specified. Its form depends on the molecule attachment mechanism. For crystal nucleation in melt or glass, A_i is usually written as

$$A_i = bD\lambda^{-2} i^{2/3} \exp\{-(W_{i+1} - W_i)/2kT\}, \qquad (3)$$

where D is the interfacial diffusion coefficient, $b = 24$ a geometrical factor, and λ the jump distance in the parent phase. Since monomer depletion is negligible during the early (nucleation) stage of the process,[29] a no-depletion boundary can be applied for the monomers, $N_1 = N_0 \exp\{-W_1/kT\}/\nu_m = \mathrm{const}$, where N_0 and ν_m are the Avogadro's number and the molar volume. Note that in the liquid the monomers dominate, thus $N_L = N_0/\nu_m \cong N_1$, which is recovered if the self-consistency criterion for cluster free energy, $W_1 = 0$, is satisfied.

The nucleation rate (net formation rate of critical fluctuations in unit volume) can be expressed as $J_{i*} = A_{i*} = N_{i*} - D_{i*+1} N_{i*+1}$. Having D, λ, and W_i fixed, transformation kinetics can be computed. In applying the classical kinetic approach to crystallization, W_i is usually taken from the ''droplet'' model, which assumes a mathematically sharp interface, yielding $W_i = -i\Delta\mu + a i^{2/3}\gamma_\infty$. Here $\Delta\mu$ is the chemical potential difference between the bulk liquid and solid, γ the free energy of the crystal/liquid interface, $a = (36\pi\nu^2)^{1/3}$, and ν the molecular volume, while the nucleation barrier and the size of the critical fluctuation are $W_{i*} = (16\pi/3)\gamma^3(\Delta\mu/\nu)^{-2}$ and $R^* = 2\gamma(\Delta\mu/\nu)^{-1}$, respectively. [Note, that $(4\pi/3)R^{*3} = i^*\nu$.] The interfacial diffusion coefficient D that describes molecule transfer across the interface is usually approximated by that of the liquid, which is customarily evaluated from the viscosity via the Stokes–Einstein relationship.

The numerical solution obtained under typical conditions indicates (Fig. 1) that quenching the monomer dominated initial cluster distribution (characteristic to temperatures above the melting point) to the undercooled state, a steady-state cluster population develops gradually, which ensures a constant formation rate of critical fluctuations, that drives the system from the metastable liquid/glassy state into the stable crystalline phase. The respective time-dependent nucleation rate $J(t)$ and number density of supercritical particles $N(t)$ are shown in Fig. 2. After a transient period, the number density of the supercritical clusters increases linearly with time, $N(t) \approx C + J_{\mathrm{ss}} t$, where J_{ss} is the steady-state nucleation rate. The induction time θ is evaluated by extrapolating this linear portion of $N(t)$ to zero, yielding $\theta = -C/J_{\mathrm{ss}}$.

Unfortunately, the interfacial free energy is difficult to measure independently of nucleation, and doubts were ex-

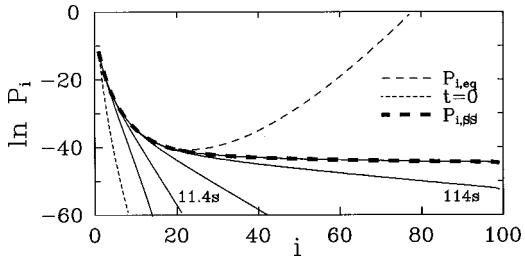

FIG. 1. Time evolution of the cluster population the classical kinetic approach predicts for lithium–disilicate at 750 K after quenching the monomer dominated initial cluster distribution characteristic to $T>T_f$. Note that $P(i)=N_i/N$, where N is the number of molecules in the system. The solid lines from left to right correspond to $t=3.8$, 11.4, 38, 114, and 380 s. For comparison, the initial (short-dashed line), the equilibrium ($P_{i,\mathrm{eq}}$—medium dashed line), and the steady state cluster probabilities ($P_{i,\mathrm{SS}}$–heavy dashed line) are also shown. The free energy of clusters was calculated using the droplet model. (The physical properties given in Ref. 29 have been adopted.)

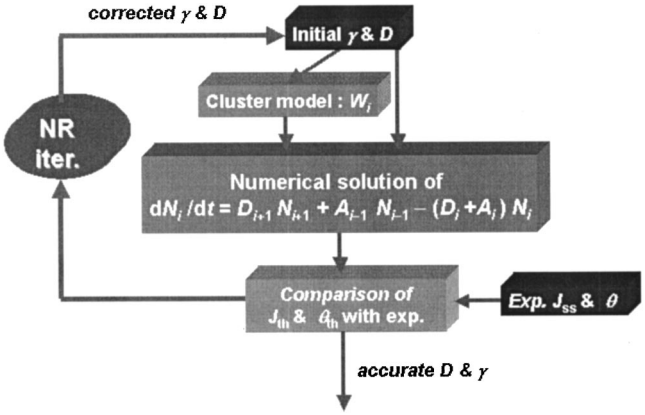

FIG. 3. Flow chart of the iteration procedure used to evaluate the interfacial free energy and interfacial diffusion coefficient from measured induction times θ and steady-state nucleation rates J_{SS}.

pressed concerning the applicability of the Stokes–Einstein relationship for highly undercooled liquids.[30] Circumventing these difficulties, Kelton and Greer performed an internal consistency test of the classical kinetic approach.[28] They evaluated γ and D from the measured induction time and steady-state nucleation rate as a function of temperature. Using these temperature dependencies, they predicted the number density of supercritical clusters for multistage heat treatments. They reported a good agreement with experiments performed on lithium–disiliciate, indicating that the classical approach is able to describe the dynamics of near critical clusters with rate coefficients evaluated from nucleation experiments that probe such microclusters.

To obtain the possibly most reliable estimate of the interfacial free energy of critical clusters, we follow the approach by Kelton and Greer.[28] We evaluate D and γ from the measured induction times and steady-state rates. The flow chart of this rather complex procedure is shown in Fig. 3. First, we chose reasonable starting values for D and γ, these and the droplet model are used to calculate the rate coefficient A_i and D_i of the master equations. The governing equations are then solved numerically, providing theoretical results for θ and J_{ss}, which are compared with their experimental counterparts. If the relative differences $|\theta-\theta_{\mathrm{exp}}|/\theta_{\mathrm{exp}}$ and $|J_{\mathrm{ss}}-J_{\mathrm{ss,exp}}|/J_{\mathrm{ss,exp}}$ are larger than a prescribed value (10^{-8}), Newton–Raphson iteration is used to improve the values for D and γ. This procedure is repeated until *both* the relative differences become less than 10^{-8}.

Note that the results of this procedure depend on the cluster model applied: One is able to calculate the transient effects if the excess free energy W_i is known for all cluster sizes. Unfortunately, in the advanced models only the critical fluctuations can be obtained with relative ease (as nontrivial time independent solutions for the variational problem). To obtain the properties of the sub- and supercritical clusters one has to solve the far more complex time-dependent problem. To avoid this laborious approach, we use the droplet model in the fitting procedure described above. This is justified by a recent study of us, which showed that the outcome of such fitting procedure is only weakly dependent on the cluster model.[31] Results supporting this statement are presented in the Appendix.

In our numerical calculation, we used $u=1000$ for the maximum cluster size. This considerably exceeds the number of molecules (formula units) i^* in the critical fluctuations, which varied between 14 and 44 in our calculations. The results, including the steady-state nucleation rate and the induction time, are independent of the choice of u so far as $u \gg i^*$, a condition satisfied here.

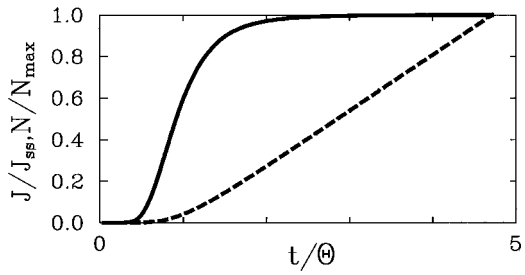

FIG. 2. Normalized nucleation rate (solid line) and number density of supercritical particles (dashed line) vs time for the system shown in Fig. 1 ($\theta=80.7$ s).

B. Cahn–Hilliard theory of crystal nucleation

For the sake of simplicity, we rely on a single-order-parameter model based on the density functional approach by Shih *et al.*[32] We assume that the excess free energy of the inhomogeneous system can be calculated as

$$W_{\mathrm{CH}}=\int d\boldsymbol{r}^3\{\Delta\omega[m(\boldsymbol{r})]+c(\nabla m)^2\}, \tag{4}$$

where the grand potential density has the simple form $\Delta\omega=\xi m^2(1-m)^2+\eta m$, m is a structural order parameter that can be interpreted as the normalized Fourier amplitude of the dominant density waves used in expanding the free energy functional.[32] The first term of $\Delta\omega$ follows from a Ginzburg–Landau expansion performed in equilibrium for the bcc structure in terms of the amplitude of the (110) static density waves.[32] Since we are concerned with more complex crystal structures, this term should be viewed as a suitably param-

eterized phenomenological relationship. There are various ways to make the generalization for the undercooled state. Here, following Harrowell and Oxtoby,[33] we add a second term ηm to the grand potential difference, a form that proved suitable for quantitatively describing the ice nucleation in undercooled liquid water.[20] Evidently, η should be chosen so that the difference between the minima of $\Delta\omega$ be equal to the experimentally determined volumetric Gibbs free energy difference $\Delta g=\Delta\mu/\nu$ between the liquid and solid. The physical meaning of the other model parameters is also clear (at least for bcc structure): $\xi=6\rho_0 kT/S(K_{110})$ and $c=-1/2\rho_0 kTC''(K_{110})$,[32] where ρ_0, $S(K_{110})$, and $C''(K_{110})$ are the density of the initial liquid state, the structure factor of the liquid, the second derivative of the two-particle direct correlation function ($C=1-1/S$) of the liquid, where the latter are evaluated at the first neighbor reciprocal lattice vector K_{110} of the crystal. Following previous work, we assume that ξ and c do not depend on temperature, which is certainly reasonable for small undercoolings ($T\approx T_f$). Note that this assumption may prove a rough approximation at large undercoolings. Molecular dynamics simulations are underway to clarify the validity range of these assumptions.

The critical fluctuation (nucleus) represents a saddle point of the W_{CH} functional. The respective $m(\boldsymbol{r})$ emerges as a nontrivial solution of the Euler–Lagrange equation $0=\partial\Delta\omega/\partial m-2c\nabla^2 m$ under boundary conditions $m\to m_0$ for $|\boldsymbol{r}|\to\infty$ and $\nabla m\to 0$ for $|\boldsymbol{r}|\to 0$, where $m_0=0$ is the order parameter of the supersaturated liquid. Assuming spherical symmetry (reasonable approximation considering the weak anisotropy of γ),[3–5] the Euler–Lagrange equation reduces to an ordinary differential equation. It has been solved here by a variable fourth/fifth order Runge–Kutta method. Inserting the solution into Eq. (4), one obtains the excess free energy W^*_{CH} of the critical fluctuation. Equating this quantity with the classical expression W_{i*}, one obtains the interface free energy of the cluster as $\gamma=(3\Delta g^2 W^*_{\mathrm{CH}}/16\pi)^{1/3}$. Note that this is the quantity that is usually evaluated from nucleation experiments via procedures akin to the one described in the previous subsection.

Inversely, one may use the temperature dependent interface free energy data to fix ξ and c. In this work the nonlinear least square method is used to fit ξ and c to the $\gamma(T)$ relationships deduced from nucleation experiments as described in Sec. II A.

C. Interfacial properties

Once the Cahn–Hilliard parameters ξ and c are determined, the properties of the *equilibrium planar interface*, such as the interface free energy and the 10%–90% thickness (the distance on which m varies between 0.1 and 0.9) can be calculated directly: $\gamma_\infty=(c\xi)^{1/2}/3$ and $d=4a\tanh(0.8)\times(c/\xi)^{1/2}$.[20,22] The latter follows from the fact that for planar geometry the order parameter varies as $m(z)=1/2[1+\tanh(-z/z_0)]$ across the interface, where $z_0=2(\xi/c)^{1/2}$, while z is the perpendicular distance from the interface.

Other interfacial properties of interest are those that describe the curvature dependence of the interfacial free energy. The curvature effect is well known for liquid droplets. In the thermodynamic description by Tolman,[34] the phenomenon is formulated in terms of the Tolman length $\delta_T=R_e-R_p$,[35] (the distance of the equimolar surface[36,37] and the surface of tension[37,38]) as

$$\gamma\approx\gamma_\infty/(1+2\delta_T/R_p), \tag{5}$$

a relationship based on a hypothesized constancy of δ_T. While a rigorous derivation of these notions for crystalline particles is unavailable, a quantity analogous to δ_T has already been evaluated from computer simulations.[39] Here we derive the Tolman-length in four ways:

(i) Via a ''liquid droplet'' approximation, where the radius of the equimolar surface is replaced by that for the Gibbs surface of the order parameter profile R_m, and the expression $R_p=[3W^*/(2\pi\Delta g)]^{1/3}$ deduced for liquid droplets is adopted for the surface of tension.
(ii) Following the treatment of Fisher and Wortis[40] valid for the equilibrium planar interface, for symmetric order parameter profiles (as in our case), the Tolman length is zero.
(iii) On the basis of Eq. (5), however, with R_m as the radius of the cluster [$\delta_1=1/2R_m(\gamma_\infty/\gamma-1)$].
(iv) (iii) On the basis of Eq. (5) [$\delta_2=1/2R_p(\gamma_\infty/\gamma-1)$].

While definitions (i) and (ii) are exact so far as the liquid droplet approximation is justified, (iii) and (iv) rely on the hypothesized constancy of the Tolman length. (iii) and (iv) are calculated here for the sake of comparison with an analog quantity evaluated from computer simulations.[39]

In addition, we investigate the temperature dependence of a ''characteristic interface thickness'' δ_{DIT} defined as the relative shift of the interfacial enthalpy and entropy profiles in a recent phenomenological diffuse interface theory of nucleation (DIT).[18] Assuming that this quantity is independent of size, the DIT leads to a remarkable agreement with experiments on vapor condensation[18] and crystal nucleation[18] including fcc nucleation in the hard sphere system,[41] and with molecular dynamics simulations.[42] An exception is ice nucleation,[43] where a temperature dependent δ_{DIT} that decreases toward its equilibrium value $\delta_{\mathrm{DIT,eq}}=\gamma_\infty/\Delta h(T_f)$ with increasing temperature had to be introduced to ensure agreement with experiments ($\Delta h>0$ is the volumetric enthalpy difference). δ_{DIT} is related to the free energy of critical fluctuations as $\delta_{\mathrm{DIT}}=[3W^*/(4\pi\Delta g\psi)]^{1/3}$, where ψ is a function of $\eta=\Delta g/\Delta h$,[18] defined in the Appendix.

Our main concern is whether either the Tolman length or the characteristic thickness may be considered constant (independent of temperature) as hypothesized in previous work, possibilities that could enormously reduce the theoretical difficulties associated with computing the curvature correction.

III. PHYSICAL PROPERTIES

The abilities of the method described in the previous section are first demonstrated in two cases (Lennard-Jones

TABLE I. Physical properties of mLJ Ar.

Symbol	Unit	
M	g	39.948
ρ_S	kg/m^3	1694.7
λ	Å	3.3954
γ_∞	mJ/m^2	5.79 ± 0.17
T_f	K	83.75
ΔH_f	J/mol	1141.9
$\Delta C_p = \Sigma C_i T^i$	J/mol/K	
C_0		8.727 69
C_1[a]		$9.819\,15 \times 10^{-2}$
C_2		$-3.326\,96 \times 10^{-3}$
C_3		7.4817×10^{-5}
C_4		$-5.850\,48 \times 10^{-7}$
$D = D_0 \exp(-D_1/T)$		
D_0	m^2/s	4.91×10^{-8}
D_1	K	287.847

[a]C_i were obtained by least square fitting to $\Delta C_p(T)$ from Ref. 44.

system and ice nucleation in undercooled water) where interfacial properties are known either from computer simulations or experiments.

The relevant physical properties of the bulk solid and liquid phases and of the solid–liquid interface of the modified Lennard-Jones (mLJ) system introduced by Broughton and Gilmer are known from extensive molecular dynamics simulations (see Table I).[44] The nucleation rate free of annealing effects has been determined by extrapolation to $T^* = 0.45$ by Báez and Clancy.[39] The usual dimensionless Lennard-Jones quantities were transformed to dimensional ones using $\sigma = 3.383$ Å, $\epsilon = 137.07\,k$, and $m = 6.634 \times 10^{-26}$ kg chosen so that the mLJ data reproduce the density and the vapor–liquid surface tension of argon at its triple point, where σ, ϵ, and m are the length and energy scales of the LJ potential, and the molecular mass.

The physical properties of the hexagonal ice (I_h)–water system and their sources are summarized in Table II and Ref. 20. Nucleation rates Taborek obtained[45] on emulsion samples have been selected, as they are shown to refer to volume nucleation, and they are the lowest of the experimental data,[43] increasing the probability that they refer indeed to homogeneous nucleation.

TABLE II. Physical properties of the ice-water system.

Symbol	Unit	
M	g	18.02
ρ_S	kg/m^3	917
λ	Å	2.76
γ_∞	mJ/m^2	29.1 ± 0.8
T_f	K	273.15
ΔH_f	J/mol	6019
$\Delta C_p = \Sigma C_i T^i$ $T > 232$ K	J/mol/K	
C_0		82 243.06
C_1		-1212.111
C_2		6.703 77
C_3		$-1.647\,88 \times 10^{-2}$
C_4		$1.518\,75 \times 10^{-5}$
$\log(D\ \mathrm{s/m^2}) = \Sigma D_i T^i$		
D_0		-1358.196
D_1		28.1413
D_2		$-0.233\,151$
D_3		$9.576\,40 \times 10^{-4}$
D_4		$-1.949\,37 \times 10^{-6}$
D_5		$1.573\,05 \times 10^{-9}$

The oxide glasses have particular advantages for nucleation studies. In glass forming melts, both nucleation and crystal growth occur relatively slowly because of the high viscosities involved (typically 10^6–10^{12} Pa s). Also, crystallization can be arrested by fast cooling. Accordingly, demonstration of volume nucleation is simple, as opposed to the laborious methods needed in the case of undercooled liquid emulsions. Consequently, nucleation and growth rates can be conveniently and accurately determined after high temperature treatments by fast cooling to room temperature and utilizing quantitative optical microscopy. While most glasses show crystal nucleation initiated by heterogeneities at the external surfaces, and it is necessary to add a nucleating agent (e.g., metallic particles) to promote heterogeneous nucleation in the volume; certain oxide systems, including ''simple'' stoichiometric glass compositions (where the crystallizing phase has the same compositions as the parent glass), were found to exhibit volume nucleation without nucleating agents.

The steady-state nucleation rates measured on stoichiometric glasses show the familiar ''bell shape'' as a function of temperature. The maximum nucleation rates vary between 1.9×10^{12} m^{-3} s^{-1} for barium–disilicate glass to 1.7×10^6 m^{-3} s^{-1} for wollastonite glass, the latter being near the lower limit of detection. The consistent pattern of these results and the extreme undercooling required for nucleation indicate a predominantly homogeneous nucleation. Supporting evidence for homogeneous nucleation is also given by the close similarities of J data from various investigators studying the same system,[11,46] and by a work, which excluded heterogeneous nucleation on Pt particles, a mechanism suspected earlier.[11] Glasses made from ordinary purity batch were compared with those from extremely high purity starting materials, and showed no differences in nucleating behavior.[11] Considering these features, the analysis of the classical kinetic approach is performed on stoichiometric oxide glasses. These substances have the further advantage that, due to the lack of chemical diffusion, the thermodynamics of crystallization is far simpler than for off-stoichiometric compositions.

Five stoichiometric oxide glasses that show volumetric nucleation [barium–disilicate—$BaO \cdot 2SiO_2$ (BS_2); lithium–disilicate—$Li_2O \cdot 2SiO_2$ (LS_2); wollastonite—$CaO \cdot SiO_2$ (CS); and two soda–lime–silica compositions $Na_2O \cdot 2CaO \cdot 3SiO_2$ (NC_2S_3) and $2Na_2O \cdot CaO \cdot 3SiO_2$ (N_2CS_3)] have been selected for our study. The steady-state nucleation rate and the induction time were determined by the double stage method, performing a nucleation heat treatment at a temperature where growth is negligible (nucleation stage), and growth to observable size at another temperature, where nucleation is negligible (growth stage). θ and J_{ss} were evaluated from the time dependent number density of observable crystallites which, to a good accuracy, is proportional with the number density of critical particles formed during the nucleation stage. Thus, θ deduced for the observable par-

TABLE III. Physical properties of glasses used in the calculations.

Composition		LS_2	BS_2	NC_2S_3	N_2CS_3	CS
Molar mass	M (g)	150.05	273.5	354.4	360.29	116.16
Mass density	ρ_m (g/cm^3)	2.452[a]	3.729[a]	2.80[a]	2.76[a]	3.09[a]
Jump distance	λ (Å)	4.7	4.96	5.95	6.08	3.97
Heat of fusion	ΔH_f (kJ/mol)	61.1[b]	37.5[d]	86.2[e]	64.9[f]	62.1[h]
Melting temperature	T_f (K)	1307[b]	1693[d]	1564[e]	1448[g]	1767[h]
Specific heat difference:	C_0 (J/mol K)	−7.3846[c]	9.86[c]	43.29[e]	−71.379*[g]	63.607[c]
$\Delta C_p = C_0 + C_1 T + C_2 T^2$	C_1	1.969×10^{-2} [c]			0.103 22*[g]	-3.0122×10^{-2} [c]
$*\Delta C_p = C_0 + C_1 T + C_2/T$	C_2				5 652 584*[g]	9.6693×10^{-6} [c]

[a]Reference 47.
[b]Reference 48.
[c]Reference 12(a).
[d]Reference 49.
[e]Reference 50.
[f]Reference 51.
[g]Reference 52.
[h]Reference 12(c). $\lambda = \nu^{1/3}$ is used.

ticles is essentially equal to that for nucleation. Details and difficulties of this method have been discussed elsewhere.[11]

To ensure the possible highest accuracy in the test, critically assessed thermodynamic properties (listed in Table III) have been used.[12,47–52] For example, in the case of lithium–disilicate the Gibbs free energy and other thermodynamic functions have been evaluated by fitting polynomials to the experimental data of Takahashi and Yoshio.[48] This procedure assigns 52.7 kJ/mol for the room temperature heat of crystallization, in excellent, agreement with the experiments (53.5 ± 4 kJ/mol) by Sen *et al.*[53] (The data by JANAF[54] indicate less than 45.1 kJ/mol for the same temperature.)

The experimental nucleation rate and induction time data were taken from the following sources: LS_2 (Ref. 55), BS_2 (Ref. 56), N_2CS_3 (Ref. 57), NC_2S_3 (Ref. 50), and CS [Ref. 12(c)].

IV. RESULTS AND DISCUSSION

A. Test of the Cahn–Hilliard analysis

1. Modified Lennard-Jones system

As a first test, we evaluate the 10%–90% interface thickness from the single nucleation rate value available for the modified Lennard-Jones system. Here the interface free energy γ_∞ is known at the melting point, thus the knowledge of the nucleation rate at a single temperature is enough to determine the Cahn–Hilliard (CH) parameters ξ and c. The interfacial free energy evaluated from the nucleation rate of Báez and Clancy (which is free from annealing effects),[39] is substantially smaller than γ_∞ [Fig. 4(a)], indicating a positive temperature coefficient for the interface free energy, as seen in experiments on various liquids and glasses. The respective 10%–90% thickness, $d = 2.98\sigma$, is in an excellent agreement with those from molecular dynamics simulations ($\sim 3\sigma$),[2,3] indicating that the CH approach is consistent with exact result from computer simulations. The Cahn–Hilliard prediction for γ increases monotonically with temperature. This apparent temperature dependence follows from the curvature dependence of γ. (Note that the critical size increases with decreasing undercooling.) The radial order parameter—and grand potential density profiles [Figs. 4(b) and 4(c)] indicate that at the nucleation temperature one cannot find bulk crystal properties even at the center of the critical fluctuations. The Tolman length evaluated by methods (i), (iii), and (iv) is strongly size dependent [decreases with increasing size, see Fig. 4(d)], as seen in computer simulations,[39] and indeed converges to zero at small undercoolings (for large particles). The characteristic interface thickness of the DIT, in turn, shows only weak size dependence despite the lack of bulk properties at the center of fluctuations.

2. Ice-water system

A further test of the approach we propose can be performed on ice nucleation, where the nucleation rate is known for several temperatures. Here the transient time is too short to be measured. Therefore, we use the diffusion coefficient of

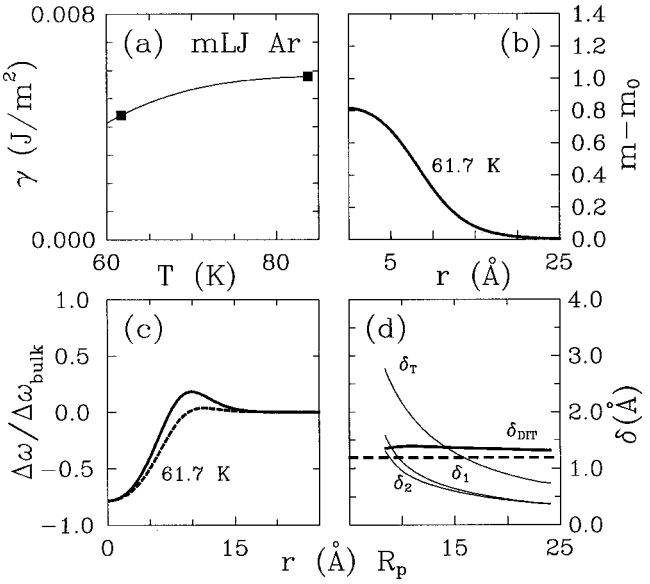

FIG. 4. Testing of the Cahn–Hilliard analysis on the modified Lennard-Jones system, where the interface free energy is known (see Ref. 3). (a) Interface free energy vs temperature. The value from molecular dynamics at the melting point (Ref. 3), and the one evaluated from the nucleation rate (Ref. 39) observed in molecular dynamics are denoted by full squares. For comparison, the temperature dependence obtained with the respective Cahn–Hilliard parameters ξ and c is also shown (solid line). (b) Radial order parameter profile. (c) Radial grand potential density profiles: Solid line—$\Delta\omega[m(\mathbf{r})] + c(\nabla m)^2$; dashed line—local contribution, $\Delta\omega[m(r)]$. (d) Curvature parameters: Tolman lengths determined following routes (i), (iii), and (iv) (δ_T, δ_1, and δ_2); and the characteristic interface thickness vs radius of the surface of tension R_p calculated using ξ and c (δ_{DIT}). For comparison, the melting point value of δ_{DIT} is also presented (dashed line).

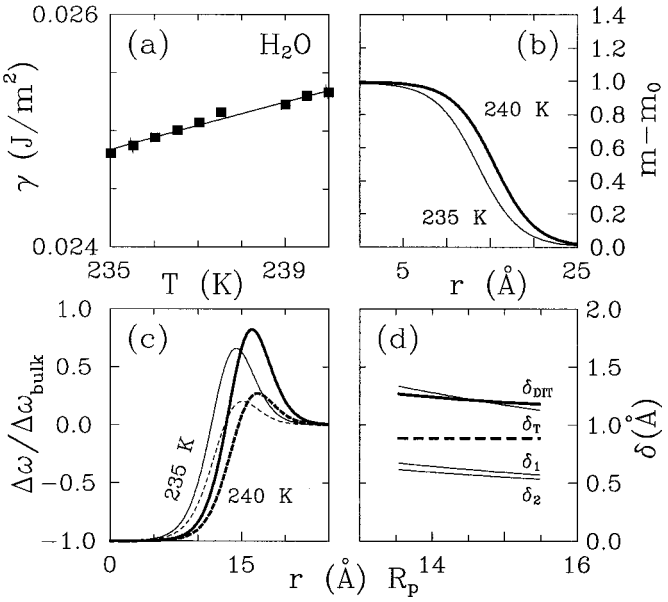

FIG. 5. Testing of Cahn–Hilliard analysis on the ice-water system, where the interface thickness (Ref. 59) and interface free energy (Ref. 60) are known. (a) Interface free energy vs temperature evaluated from nucleation rates measured by Taborek (Ref. 44) (full squares). The temperature dependence obtained with the best fit Cahn–Hilliard parameters ξ and c is also shown (solid line). (b) Radial order parameter profile. (c) Radial grand potential density profiles: Solid line—$\Delta\omega[m(\boldsymbol{r})]+c(\nabla m)^2$; dashed line—local contribution, $\Delta\omega[m(r)]$. Heavy and light lines in panels (b) and (c) indicate profiles corresponding to the upper and lower limits of the temperature range. (d) Curvature parameters: Tolman lengths determined following routes (i), (iii), and (iv) (δ_T, δ_1, and δ_2); and the characteristic interface thickness vs radius of the surface of tension R_p calculated using ξ and c (δ_{DIT}). For comparison, the melting point value of δ_{DIT} is also presented (dashed line).

undercooled water determined experimentally. The interface free energies evaluated from the nucleation rate data, and the $\gamma(T)$ relationship obtained with the best fitting Cahn–Hilliard parameters indicate again a positive temperature coefficient [Fig. 5(a)]. The thickness $d=9.7\pm0.4$ Å obtained for the equilibrium planar interface is comparable to the 10%–90% thickness from experiment (10.0 Å)[58] and from molecular dynamics simulations for the translational order profiles (8.6 and 9.9 Å for the prism and basal planes, respectively).[59] While this coherence is reassuring, the comparison of the interface free energy $\gamma_\infty=27.1\pm0.2$ mJ/m^2 with independent experimental data is hardly conclusive due to a considerable scatter of the latter (Table IV).[60] The variation of the independent data might be attributed to the uncertainties of the specific methods used to obtain them. Considering the associated difficulties (see Sec. IV C and Ref. 61), probably Hardy's high precision data are the most reliable.

TABLE IV. The free energy of the I_h/water interface at $T\approx T_f$.

Method	γ(mJ/m^2)	Reference
Shape of grain boundary groove	44 ± 10	60(b)
Contact angles (Young equation)	33 ± 3	60(d)
Crystal growth	32 ± 2	60(a)
Freezing in porous medium	31.7 ± 2.7	60(g)
Shape of grain boundary groove	29.1 ± 0.8	60(c)
Growth velocity of dendrites	28	60(f)
Morphological instability	25	60(e)

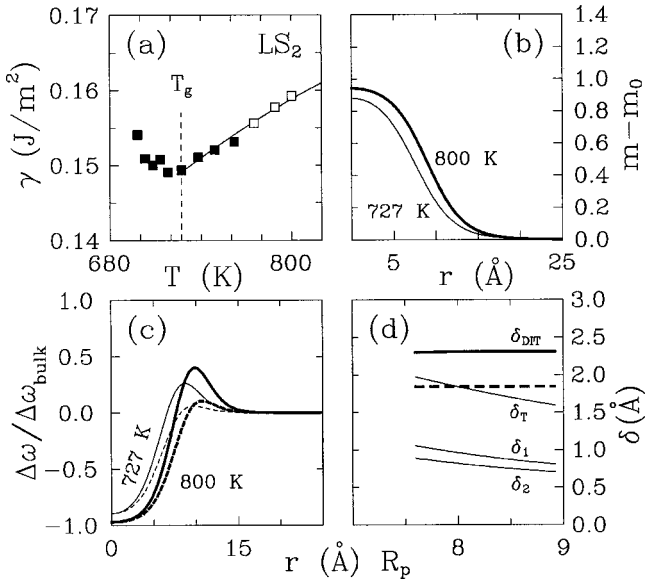

FIG. 6. Cahn–Hilliard analysis of experimental nucleation rates in lithium disilicate. Notation as in Fig. 5.

Throughout the temperature range covered by experiment, we find bulk crystal properties at the center of critical fluctuations [Figs. 5(b) and 5(c)]. Both the Tolman length and δ_{DIT} shows a pronounced decrease with increasing size/temperature [Fig. 5(d)]. Such dependence of δ_{DIT} has been noted in previous work and was associated with structural changes of the undercooled water.[45]

Considering these, we may conclude that the interfacial properties obtained via the Cahn–Hilliard analysis of nucleation experiments are not inconsistent with interfacial information from independent sources.

B. Application to oxide glasses

The results of the Cahn–Hilliard analysis of nucleation data on five stoichiometric oxide glass compositions are summarized in Figs. 6–10 and Table V. In agreement with previous work,[10,11,12(c),55,57] the interfacial free energy of critical fluctuations follows a qualitatively similar temperature dependence for all substances studied here. A minimum is seen close to the glass transition temperature, which merges into a nearly linear temperature dependence at higher temperatures [see Figs. 6(a)–10(a)]. The origin of this minimum is unclear. It is probably associated with the changing time scale of structural relaxation near glass transition T_g. Since such effects as that of frozen-in (static) density fluctuations on nucleation[62] are expected to occur near to or below T_g, we apply the Cahn–Hilliard analysis to only higher temperatures ($T>T_g$), where the $\gamma(T)$ relationship is close to linear. Note that due to the extreme measurement times following from the low nucleation rates, the linear behavior expected at high temperatures has not been fully established for NC_2S_3 and CS, therefore, here the asymptotic behavior of $\gamma(T)$ determined by the highest temperature points were used in the analysis.

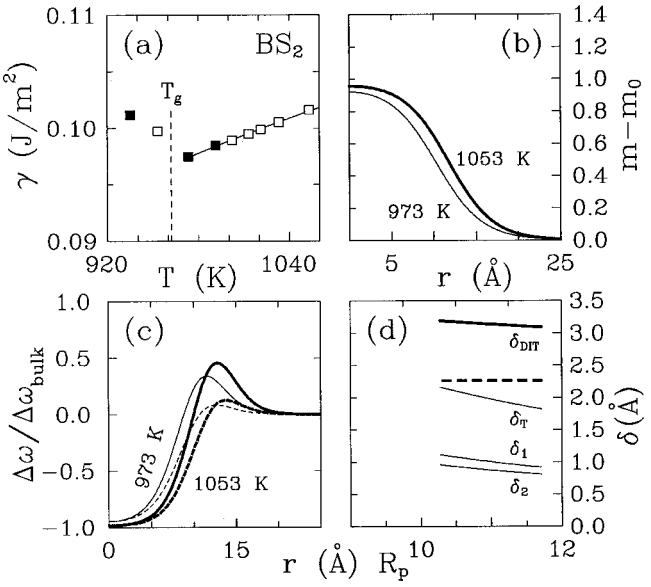

FIG. 7. Cahn–Hilliard analysis of experimental nucleation rates in barium disilicate. Notation as in Fig. 5.

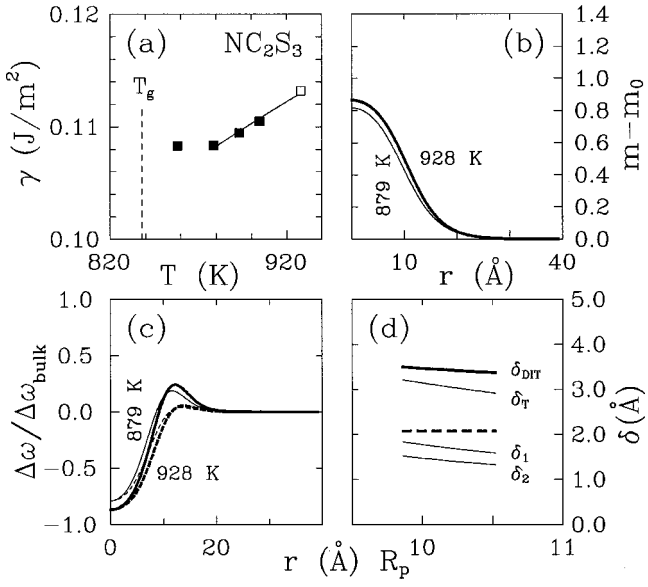

FIG. 9. Cahn–Hilliard analysis of experimental nucleation rates in a soda–lime–silica glass of stoichiometry 1:2:3. Notation as in Fig. 5.

The normalized interfacial free energy $\alpha = \gamma_\infty N_0 \nu^{2/3}/\Delta H_f$ (often called Turnbull's α) and interface thickness $\beta = d/\nu^{1/3}$ deduced from the best fitting Cahn–Hilliard parameters ξ and c fall in the ranges $0.27 < \alpha < 0.51$ and $1.7 < \beta < 4.0$, respectively, while $8.3\,\text{Å} < d < 15.6\,\text{Å}$. These data are comparable to exact results from molecular dynamics simulations for other systems[3–5,63] (see Table V). The order parameter and grand potential density profiles indicate that bulk or nearly bulk crystal properties exist at the center of critical fluctuations in LS_2 and BS_2, while considerable deviation from the bulk properties (ramified cluster) is observed for the rest of the compositions [see Figs. 6(b) and 6(c)–10(c)]. In all cases the Tolman length decreases with increasing size of the fluctuation [Figs. 6(d)–10(d)]. In a few cases we have verified numerically that indeed $\delta_T \to 0$ for $R_p \to \infty$ (as follows from the theorem of Fisher and Wortis). The characteristic interface thickness δ_{DIT} shows a weak temperature dependence (decreases with increasing T) for BS_2 and NC_2S_3, while it is apparently constant (at least in the rather limited temperature ranges we investigated) for the rest of the compositions [Figs. 6(d)–10(d)]. It is, however, larger than $\delta_{DIT,eq} = \gamma_\infty/\Delta h(T_f)$ for all substances, if γ_∞ from the Cahn–Hilliard analysis is used. This indicates that the DIT and CH approaches are not mutually consistent.

C. Discussion

Before addressing the implications of the interface properties we obtained, let us briefly review previous information on these quantities.

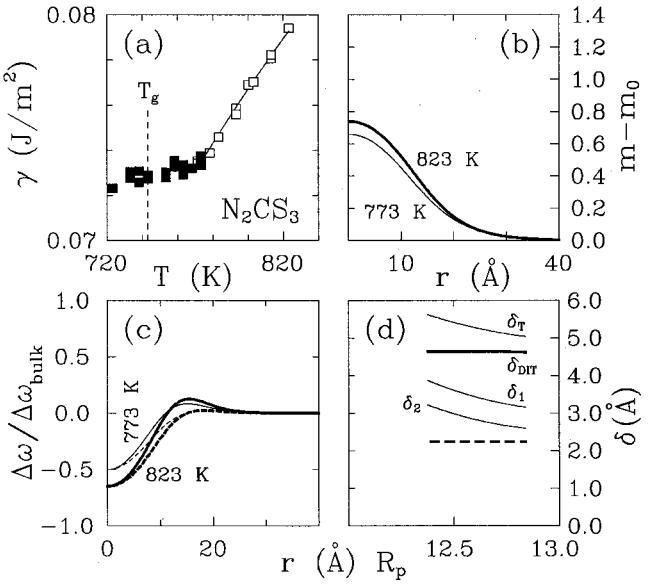

FIG. 8. Cahn–Hilliard analysis of experimental nucleation rates in a soda–lime–silica glass of stoichiometry 2:1:3. Notation as in Fig. 5.

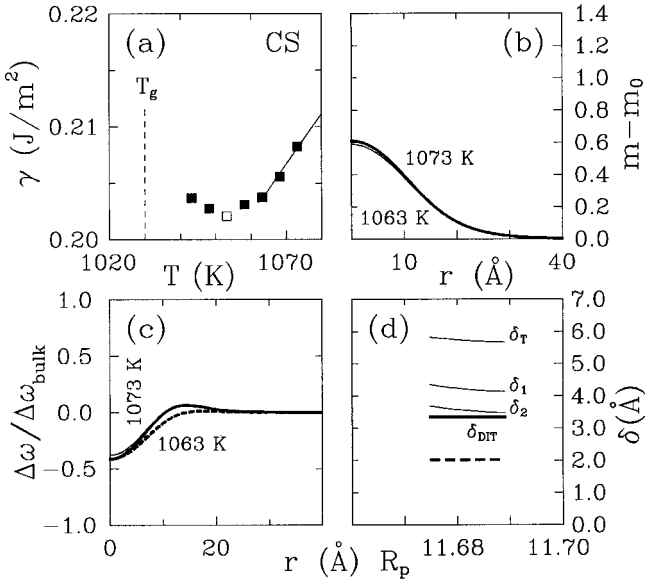

FIG. 10. Cahn–Hilliard analysis of experimental nucleation rates in wollastonite glass. Notation as in Fig. 5.

TABLE V. Interfacial properties from the Cahn-Hilliard analysis and molecular dynamics simulations.

Composition	γ_∞ (mJ/m^2)	α	α_a	d (nm)	β	β_a
mLJ Ar	5.8±0.2[a]	0.352±0.010[a]	0.352±0.010[a]	1.01±0.06	2.97±0.17	2.97±0.17
H_2O	27.1±0.2	0.277±0.002	0.400±0.003	0.97±0.04	3.04±0.12	4.38±0.17
LS_2	183.9±3.5	0.395±0.008	0.822±0.016	0.83±0.05	1.78±0.10	3.70±0.20
BS_2	115.5±0.9	0.456±0.004	0.912±0.007	1.02±0.02	2.07±0.04	4.14±0.08
N_2CS_3	111.3±1.8	0.373±0.006	0.959±0.016	1.64±0.04	2.73±0.07	7.02±0.17
NC_2S_3	141.5±2.4	0.349±0.006	0.879±0.015	1.18±0.04	1.98±0.07	4.99±0.18
CS	331.9±3.9	0.507±0.006	0.867±0.010	1.56±0.03	3.94±0.06	6.74±0.11
HS	⋯	0.51[b]	0.51[b]	⋯	3.1–3.3[c]	3.1–3.3[c]
Ni	326[d]	0.58[d]	0.58[d]	⋯	⋯	⋯

[a]Molecular dynamics data from Ref. 3.
[b]Molecular dynamics data from Ref. 4.
[c]Molecular dynamics data from Ref. 62.
[d]Molecular dynamics data from Ref. 5.

The reduced interface free energy $\alpha=\gamma N_0 \nu^{2/3}/\Delta H_f$ has been thought to depend on the crystal structure only. In the pioneering experiments of Turnbull the elements grouped into two classes: close packed ($\alpha\approx 0.46$) and open structures ($\alpha\approx 0.33$). However, larger undercoolings have been achieved in later experiments that lead to a considerable increase and scatter of α, and spoiled this classification. While the undercooling experiments are subject to various uncertainties (heterogeneous nucleation, etc.), the most reliable information originates from the grain boundary groove method (for review see Ref. 61). Owing to its complexity, this method has been applied only to a handful of substances.[64] The respective data show considerable scatter (see Table VI). More conclusive are the exact results for the fcc structure from computer simulations (see data for the mLJ and hard sphere systems, and for nickel in Table V),[3–5] which clearly indicate that the interaction potential has a considerable effect on α, even if the crystalline structure remains the same. Thus, one may only expect similar α for substances of similar crystal structure and molecular interaction.

There is far too little experimental information available on the thickness of the crystal–liquid interface to seek correlations. However, the lattice models predict that the interface thickness increases with decreasing melting entropy.[61] For example, in Temkin's multilayer lattice model $d \propto R/\Delta S_f$.[61]

It appears, however, that the reduced interface free energy α shows a considerable scatter for silicate glasses (materials that are chemically and structurally rather similar), and the reduced interface thickness β does not correlate with $R/\Delta S_f$.

It is worth recalling, however, that the oxide glasses are complex systems in which the molar volume traditionally refers to a "formula unit," e.g., $BaO\cdot 2SiO_2$, which contains several atoms. Naturally the question arises whether it is justifiable to compare these quantities with each other or with results from monatomic systems. A straightforward idea is to introduce "average" atomic quantities, which are expressed in terms of the heat of fusion/atom and volume/atom: $\alpha_a=\gamma_\infty N_0(\nu/n)^{2/3}/(\Delta H_f/n)=\alpha n^{1/3}$ and $\beta_a=d/(\nu/n)^{1/3}=\beta n^{1/3}$, where n is the number of atoms in the formula unit. Were such an approach justified, one should obtain a linear relationship when plotting α versus $n^{-1/3}$ (at least for materials with similar molecular interactions/structure). Indeed, we find a linear relationship of slope $\alpha_a=0.89\pm 0.02$ for the oxide glass compositions [Fig. 11(a)]. This suggests that, as expected, these substances belong to the same class as far as the reduced interface energy is concerned. Note that the observed deviations from this linear relationship are larger than the error of α for the individual substances, indicating real differences in structure and/or bonding.

TABLE VI. Interface free energy from grain boundary groove.

Substance	γ(mJ/m^2)	α	Reference
Succinonitrile	8.9±0.5	0.37	64(a)
Pivalic acid	2.7±0.2	0.23	64(b)
Ice-water	29.1±0.8	0.30	60(c)
Pb	76	0.92	64(c)
(Pb–Sn melt)	56.2±7.3	0.68	64(d)
Sn (Pb–Sn melt)	132.4±17.2	1.02	64(d)
Al (Al–Cu melt)	160.0±21.2	0.58	64(d)
(Al–Si melt)	168.9±22.0	0.61	64(d)
(Al–Mg melt)	149.2±19.4	0.54	64(e)
(Al–Ni melt)	171.6±20.6	0.62	64(f)
(Al–Ti melt)	174.6±20.9	0.63	64(f)

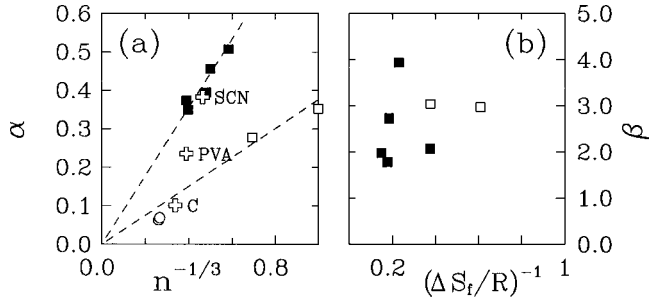

FIG. 11. Comparison of properties of the equilibrium crystal–fluid interface deduced from nucleation rates with data from other sources. (a) Reduced interface free energy vs $n^{-1/3}$; (b) reduced interface thickness vs $R/\Delta S_f$. [Filled square—oxide glass data from Cahn–Hilliard analysis; open squares—mLJ (molecular dynamics, Ref. 3) and ice-water systems (high precision datum by Hardy, Ref. 60(c)); open crosses—experimental data for succinonitrile (SCN), pivalic acid (PVA), and camphene (C); open circles—hydrocarbons ($C_{17}H_{36}$ and $C_{18}H_{38}$; data from Cahn–Hilliard analysis by L. Gránásy, unpublished).]

It is probably just coincidence that the data for mLJ Ar and H_2O seem to fall on another line of smaller slope ($\alpha_a = 0.38 \pm 0.03$). While results from a similar Cahn–Hilliard analysis of nucleation data on two hydrocarbons ($C_{17}H_{36}$ and $C_{18}H_{38}$) fall close to this line, α from direct experiments on succinonitrile and pivalic acid lie considerably higher [Fig. 11(a)]. Further work is needed to clarify whether seeking correlation with $n^{-1/3}$ has any meaning for true molecular substances such as hydrocarbons.

By contrast with the reduced interface free energy, the reduced thickness β does not show such a clear relationship to $n^{-1/3}$. It appears, furthermore, that neither β nor $\beta\, n^{1/3}$ scales with $R/\Delta S_f$ [Fig. 11(b)]. These suggest that other factors, not considered in lattice models (such as density change, layering of the liquid adjacent to crystal surface,[1–3] and surface reconstruction) also contribute to the interface thickness.

The present values for α are considerably lower that those evaluated from the same experiments using Turnbull's plot for either Gránásy's phenomenological DIT or a Cahn–Hilliard approach with double parabolic free energy.[12] The differences originate from the different temperature dependencies these models predict for the interface free energy. The coherence of the present α values seems to favor the Cahn–Hilliard approach used here (α versus $n^{-1/3}$ is rather messy for the other two models). It appears then that the $\delta_{DIT} \cong$ const, which has been used to justify the DIT approach in previous work[12,29] is just a local feature seen in the narrow temperature available for experiments, and a significant decrease of δ_{DIT} with increasing size is expected until the equilibrium value $\delta_{DIT,eq} = \gamma_\infty / \Delta h(T_f)$ [dashed line in Figs. 6(d)–10(d)] is achieved. These imply that the extra assumption that δ_{DIT} is independent of the temperature may be false. Bartell and co-workers arrived to a similar conclusion on the basis of molecular dynamics simulation of crystallization in small liquid clusters.[65] [Note that it does not influence the accuracy of the DIT for vapor condensation where only the size independence of δ_{DIT} is postulated, and the temperature dependence of δ_{DIT} is calculated from the known temperature dependencies of the surface tension and the enthalpy of evaporation. There (without using adjustable parameters) the DIT proved superior to the classical droplet model as indicated by comparison with experiment[18] and density functional theory.[66]]

An interesting limiting case from this viewpoint is crystal nucleation in the hard-sphere liquid, where the usual reduced physical properties (including the interfacial free energy, and hence δ_{DIT}) are independent of temperature. There, the height of the nucleation barrier (W^*) the DIT predicts without adjustable parameters is in an excellent agreement with Monte Carlo simulations.[41] This implies that by taking the temperature (pressure) dependence of the free energy of the planar interface into account, the accuracy of the DIT predictions for crystal nucleation could be increased.

Finally, we wish to mention that the above conclusions rest on the accuracy of α emerging from our Cahn–Hilliard analysis, which in turn depends to which extent the use of temperature independent parameters ξ and c is justifiable. This can be decided by investigating the temperature dependence of liquid structure. Molecular dynamics studies for the mLJ system are underway to address this question.

V. SUMMARY

We used the classical kinetic approach and a single-order-parameter Cahn–Hilliard model to evaluate interfacial information from nucleation data on various substances including the Lennard-Jones and ice-water system, and oxide glasses. We have shown the following.

(i) The melting point value of the reduced interface free energy (Turmbull's $\alpha = \gamma_\infty N_0 \nu^{2/3} / \Delta H_f$) varies between 0.27 and 0.51. For oxide glasses it scales with $n^{-1/3}$, and can be well approximated as $\alpha = (0.89 \pm 0.02)\, n^{-1/3}$.

(ii) In contrast with expectations based on lattice models, neither the reduced interface thickness β, nor $\beta\, n^{1/3}$ scales with $R/\Delta S_f$.

(iii) In agreement with computer simulations the Tolman length decreases with increasing cluster size. Due to the symmetric (quartic) form of the free energy–order parameter relationship adopted here, which emerges from the Ginzburg–Landau expansion by Shih *et al.*, the Tolman length tends to zero in the planar interface limit.

(iv) The characteristic interface thickness used in the phenomenological diffuse interface theory of Gránásy is constant or weakly temperature dependent in the temperature range of experiments. However, it may change significantly in broader temperature ranges, since for all substances investigated here the characteristic interface thickness exceeds considerably its planar limit $\delta_{DIT,eq} = \gamma_\infty / \Delta h(T_f)$ calculated with γ_∞ from the Cahn–Hilliard analysis.

Finally, we wish to recall that the present Cahn–Hilliard analysis relies on the constancy of parameters ξ and c, an assumption whose accuracy has yet to be assessed at large undercoolings.

ACKNOWLEDGMENTS

This work was supported by the ESA Prodex Contract No. 14613/00/NL/SFe, by the Hungarian Academy of Sciences under Contract No. OTKA-T-037323, and forms part of the ESA MAP Project No. AO-99-101.

APPENDIX: CLUSTER MODEL VERSUS NUCLEATION KINETICS

Here we compare the interfacial diffusion coefficients and interface free energies evaluated from the experimental data for the steady state nucleation rate and induction time using two different cluster models: (a) the classical droplet model (see Sec. II A), and (b) the DIT. In the latter, the work of formation reads as

$$W_i = 4\pi/3\{(R_S - \delta)^3 \Delta h - R_S^3 T \Delta s\}, \tag{A1}$$

where $R_S \approx (3i\nu/4\pi)^{1/3}$, Δh and Δs are the volumetric enthalpy and entropy densities between the bulk crystal and

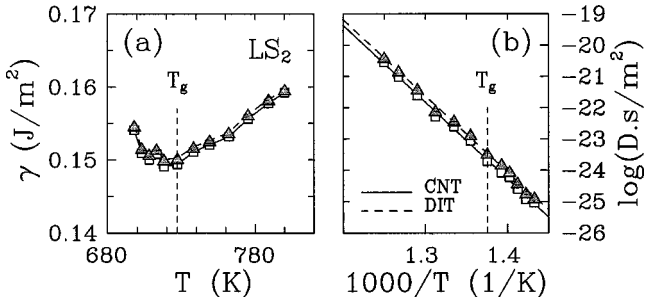

FIG. 12. Effect of cluster model on the interfacial properties evaluated from experimental induction times and steady-state nucleation rates via the method visualized in Fig. 3. (a) Interface free energy vs temperature; (b) cross-interfacial diffusion coefficient vs $1000/T$. Nucleation data measured on lithium–disilicate have been used. (Cluster models: diffuse interface theory—gray triangles; classical droplet model—empty squares.)

liquid, and δ is the characteristic interface thickness. It is assumed that bulk crystal properties exist at least in the central part of the clusters, and δ is constant regardless of size and temperature. The free energy of the critical fluctuation is $W^*_{\mathrm{DIT}}=-4\pi/3\delta^3\Delta g\psi$ and $R^*=\delta(1+q)^{1/2}\eta^{-1}$, where $\Delta g=\Delta h-T\Delta s$, $\psi=2(1+q)\eta^{-3}-(3+2q)\eta^{-2}+\eta^{-1}$, $q=(1-\eta)^{1/2}$, and $\eta=\Delta g/\Delta h$. In the DIT, W_i depends on a single interfacial parameter δ just as in the droplet model. Accordingly, only the expression for W_i needs to be replaced in the iteration procedure shown in Fig. 3, which is then aimed at determining D and δ. The corresponding interfacial free energy is $\gamma=(3\Delta g^2 W^*_{\mathrm{DIT}}/16\pi)^{1/3}$.

The diffusion coefficients and interface free energies obtained with the two cluster models are compared in Fig. 12. Only minor differences are seen in both quantities, indicating that they are rather insensitive to the choice of the cluster model.

[1] J. Q. Broughton and F. F. Abraham, Chem. Phys. Lett. **71**, 456 (1980); S. J. Cook and P. Clancy, Phys. Rev. B **47**, 7686 (1993); P. R. ten Wolde, M. J. Ruiz-Montero, and D. Frenkel, Phys. Rev. Lett. **75**, 2714 (1995).
[2] B. B. Laird and A. D. J. Haymet, Chem. Rev. **92**, 1819 (1992).
[3] J. Q. Broughton and G. H. Gilmer, J. Chem. Phys. **84**, 5749 (1986).
[4] R. L. Davidchack and B. B. Laird, Phys. Rev. Lett. **85**, 4751 (2000).
[5] J. J. Hoyt, M. Asta, and A. Karma, Phys. Rev. Lett. **86**, 5530 (2001).
[6] J. M. Howe, Philos. Mag. A **74**, 761 (1996).
[7] D. W. Oxtoby and A. D. J. Haymet, J. Chem. Phys. **76**, 6262 (1982); W. A. Curtin, Phys. Rev. B **39**, 6775 (1989); D. W. Marr and A. P. Gast, J. Chem. Phys. **99**, 2024 (1993); R. Ohnesorge, H. Löwen, and H. Wagner, Phys. Rev. E **50**, 4801 (1994).
[8] D. Turnbull, J. Chem. Phys. **18**, 768 (1950); **18**, 769 (1950); **20**, 411 (1952).
[9] D. M. Herlach, Mater. Sci. Eng., R. **12**, 177 (1994).
[10] K. F. Kelton, Solid State Phys. **45**, 75 (1991).
[11] P. F. James, *Advances in Ceramics*, edited by J. H. Simmons, D. R. Uhlmann, and G. H. Beall (American Ceramics Society, Columbus OH, 1982), Vol. 4, p. 1; P. F. James, *Glasses and Ceramics*, edited by M. H. Lewis (Chapman and Hall, London, 1989), p. 59; P. F. James, J. Non-Cryst. Solids **73**, 517 (1985).
[12] (a) L. Gránásy and F. Iglói, J. Chem. Phys. **107**, 3634 (1997); (b) L. Gránásy and P. F. James, Proc. R. Soc. London, Ser. A **454**, 1745 (1998); (c) L. Gránásy, T. Wang, and P. F. James, J. Chem. Phys. **108**, 7317 (1998).
[13] D. Turnbull and J. C. Fisher, J. Chem. Phys. **17**, 71 (1949).
[14] J. L. Schmitt, A. Zalabsky, and G. W. Adams, J. Chem. Phys. **79**, 4496 (1983); P. E. Wagner and R. Strey, *ibid.* , 5266 (1984); R. Strey, P. E. Wagner, and T. Schmeling, *ibid.* **84**, 2325 (1986); C.-H. Hung, M. J. Krasnopoler, and J. L. Katz, *ibid.* **90**, 1856 (1989).
[15] K. Binder and D. Stauffer, Adv. Phys. **25**, 343 (1974); V. A. Shneidman, K. A. Jackson, and K. M. Beatty, J. Chem. Phys. **111**, 6932 (1999).
[16] S. L. Girshick and C. P. Chiu, J. Chem. Phys. **93**, 1273 (1990); S. L. Girshick, *ibid.* **94**, 826 (1991).
[17] C. K. Bagdassarian and D. W. Oxtoby, J. Chem. Phys. **100**, 2139 (1994).
[18] L. Gránásy, J. Non-Cryst. Solids **162**, 301 (1993); Europhys. Lett. **24**, 121 (1993); J. Chem. Phys. **104**, 5188 (1996); J. Non-Cryst. Solids **219**, 49 (1997).
[19] F. Spaepen, Mater. Sci. Eng., A **178**, 15 (1994); Solid State Phys. **47**, 1 (1994).
[20] L. Gránásy, J. Mol. Struct. **485–486**, 523 (1999).
[21] L. Gránásy and D. W. Oxtoby, J. Chem. Phys. **112**, 2399 (2000); **112**, 2410 (2000).
[22] L. Gránásy, T. Börzsönyi, and T. Pusztai, J. Cryst. Growth **237-239**, 1813 (2002); Phys. Rev. Lett. **88**, 206105 (2002).
[23] K. Binder, Phys. Rev. B **15**, 4425 (1977); P. Mirold and K. Binder, Acta Metall. **25**, 1435 (1977); J. L. Spouge, Math. Proc. Cambridge Philos. Soc. **96**, 351 (1984).
[24] J. S. Langer, Ann. Phys. (N.Y.) **54**, 258 (1969).
[25] M. Grant and J. D. Gunton, Phys. Rev. B **32**, 7299 (1985).
[26] A. Roy, J. M. Rickman, J. D. Gunton, and K. R. Elder, Phys. Rev. E **57**, 2610 (1998).
[27] J. Huang, X. Zhu, and L. S. Bartell, J. Phys. Chem. A **102**, 2708 (1998); L. S. Bartell, Annu. Rev. Phys. Chem. **49**, 43 (1998); P. Santikary, K. E. Kinney, and L. S. Bartell, J. Phys. Chem. A **102**, 10324 (1998); Y. Chushak, P. Santikary, and L. S. Bartell, *ibid.* **103**, 5636 (1999); Y. Chushak and L. S. Bartell, *ibid.* **104**, 9328 (2000); H. S. Deng and J. F. Huang, J. Solid State Chem. **159**, 10 (2001).
[28] K. F. Kelton and A. L. Greer, Phys. Rev. B **38**, 10 089 (1988); A. L. Greer and K. F. Kelton, J. Am. Chem. Soc. **74**, 1015 (1991).
[29] L. Gránásy and P. F. James, J. Chem. Phys. **111**, 737 (1999).
[30] G. Tarjus and D. Kivelson, J. Chem. Phys. **103**, 3071 (1995) and references therein; U. Geyer, W. L. Johnson, S. Schneide, Y. Qiu, T. A. Tombrello, and M.-P. Macht, Appl. Phys. Lett. **69**, 2492 (1996); D. J. Stein and F. J. Spera, Am. Mineral. **81**, 284 (1996).
[31] L. Gránásy, T. Pusztai, and P. F. James (unpublished).
[32] W. H. Shih, Z. Q. Wang, X. C. Zeng, and D. Stroud, Phys. Rev. A **35**, 2611 (1987).
[33] P. R. Harrowell and D. W. Oxtoby, J. Chem. Phys. **86**, 2932 (1987).
[34] R. C. Tolman, J. Chem. Phys. **17**, 333 (1949).
[35] Tolman's original definition. A different definition is applied by several authors: $\delta_T=\lim_{R\to\infty} R_e-R_p$. In our terminology, the latter corresponds to the equilibrium Tolman length $\delta_{T,\mathrm{eq}}$.
[36] Defined by the position of a step function that has the same spatial integral and amplitude as the interfacial density profile.
[37] J. S. Rowlinson and B. Widom, *Molecular Theory of Capillarity* (Clarendon, Oxford, 1982).
[38] The surface at which the surface tension acts. It is the surface for which the generalized Laplace equation, $\Delta p_c=2\gamma/R+\partial\gamma/\partial R$ reduces to the original one; i.e., $\partial\gamma/\partial R=0$. For further details see Ref. 37.
[39] L. A. Báez and P. Clancy, J. Chem. Phys. **102**, 8138 (1995).
[40] M. P. A. Fisher and M. Wortis, Phys. Rev. B **29**, 6252 (1984).
[41] L. Gránásy and T. Pusztai (unpublished).
[42] L. Gránásy, Int. J. Non-Equilib. Process. **11**, 113 (1998).
[43] L. Gránásy, J. Phys. Chem. **99**, 14182 (1995).
[44] J. Q. Broughton and G. H. Gilmer, J. Chem. Phys. **79**, 5095 (1983).
[45] P. Taborek, Phys. Rev. B **32**, 5902 (1985).
[46] E. D. Zanotto and P. F. James, J. Non-Cryst. Solids **74**, 373 (1985).
[47] E. D. Zanotto and E. A. Müller, J. Non-Cryst. Solids **130**, 220 (1991).
[48] K. Takahashi and T. Yoshio, Yogyo Kyokaishi **81**, 524 (1973).
[49] E. G. Rowlands and P. F. James, in *The Structure of Non-crystalline Solids*, edited by P. H. Gaskell (Taylor and Francis, London, 1977), p. 215.
[50] C. J. R. González-Oliver and P. F. James, Thermochim. Acta **280/281**, 223 (1996).
[51] O. V. Mazurin, M. V. Streltsina, and T. P. Shvaiko-Shvaikovskaya, *Handbook of Glass Data*, Physical Science Data Vol. 15, Part C (Elsevier, Amsterdam, 1987), p. 99.
[52] V. I. Babushkin, G. M. Matveyev, and O. P. Mchedlov-Petrossyan, *Thermodynamics of Silicates* (Springer, Berlin, 1985), p. 202.
[53] S. Sen, C. Gerardin, A. Navrotsky, and J. E. Dickinson, J. Non-Cryst. Solids **168**, 64 (1994).
[54] *JANAF Thermochemical Tables*, 2nd ed. (U.S. Department of Commerce, National Bureau of Standards, Washington D.C., 1971).
[55] P. F. James, Phys. Chem. Glasses **15**, 95 (1974).
[56] E. G. Rowlands, PhD thesis, University of Sheffield, England, 1976.

[57] V. M. Fokin, A. M. Kalinina, and V. N. Filipovich, J. Cryst. Growth **52**, 115 (1981).
[58] D. Beaglehole and P. Wilson, J. Phys. Chem. **97**, 11053 (1993).
[59] J. A. Hayward and A. D. J. Haymet, J. Chem. Phys. **114**, 3713 (2001).
[60] Crystal growth: (a) R. Fernandez and A. J. Barduhn, Desalination **3**, 330 (1967); Shape of grain boundary groove: (b) D. R. H. Jones, Philos. Mag. **27**, 569 (1973); J. Mater. Sci. **9**, 1 (1974); (c) S. C. Hardy, Philos. Mag. **35**, 471 (1977); Contact angles: (d) W. M. Ketcham and P. V. Hobbs, *ibid.* **19**, 1161 (1969); Morphological instability: (e) S. R. Coriell, S. C. Hardy, and R. F. Sekerka, J. Cryst. Growth **11**, 53 (1971); Dendritic growth: (f) J. S. Langer, R. F. Sekerka, and T. Fujioka, *ibid.* **44**, 414 (1978); Y. Furukawa and W. Shimada, *ibid.* **128**, 234 (1993); Freezing in fine-pore cellulose acetate filter: (g) W. B. Hillig, *ibid.* **183**, 463 (1998).
[61] D. P. Woodruff, *The Solid–Liquid Interface* (Cambridge University Press, Cambridge, 1973).
[62] V. G. Karpov and D. W. Oxtoby, Phys. Rev. B **54**, 9734 (1996).
[63] R. L. Davidchack and B. B. Laird, J. Chem. Phys. **108**, 9452 (1998).
[64] (a) R. J. Schaefer, M. E. Glicksman, and J. D. Ayers, Philos. Mag. **32**, 725 (1975); (b) B. Bayender, N. Marasli, E. Cardirli, H. Sisman, and M. Gündüz, J. Cryst. Growth **194**, 119 (1998); (c) G. E. Nash and M. E. Glicksman, Philos. Mag. **24**, 577 (1971); (d) M. Gündüz and J. D. Hunt, Acta Metall. **33**, 1651 (1985); (e) M. Gündüz and J. D. Hunt, *ibid.* **37**, 1839 (1989); (f) N. Marasli and J. D. Hunt, Acta Mater. **44**, 1085 (1996).
[65] J. Huang and L. S. Bartell, J. Phys. Chem. (in press).
[66] V. Talanquer and D. W. Oxtoby, J. Phys. Chem. **99**, 2865 (1995).